

DOC-2004-Jan-152

A Study of Spin-dependent Interactions with  
Antiprotons  
*The Structure of The Nucleon*

*ASSIA Collaboration*



V.Abazov<sup>1</sup>, G.Alexeev<sup>1</sup>, M. Alexeev<sup>2</sup>, A. Amoroso<sup>2</sup>, N. Angelov<sup>1</sup>, M. Anselmino<sup>3</sup>, S. Baginyan<sup>1</sup>, F. Balestra<sup>2</sup>, V.A. Baranov<sup>1</sup>, Yu. Batusov<sup>1</sup>, I. Belolaptikov<sup>1</sup>, R. Bertini<sup>2</sup>, N. Bianchi<sup>11</sup>, A. Bianconi<sup>4</sup>, R. Birsa<sup>13</sup>, T. Blokhintseva<sup>1</sup>, A. Bonyushkina<sup>1</sup>, F. Bradamante<sup>13</sup>, A. Bressan<sup>13</sup>, M.P. Busa<sup>2</sup>, V. Butenko<sup>1</sup>, M. L. Colantoni<sup>5</sup>, M. Corradini<sup>4</sup>, S. Dalla Torre<sup>13</sup>, A. Demyanov<sup>1</sup>, O. Denisov<sup>2</sup>, E. De Sanctis<sup>11</sup>, P. Di Nezza<sup>11</sup>, V. Drozdov<sup>1</sup>, J. Dupak<sup>9</sup>, G. Erusalimtsev<sup>1</sup>, L. Fava<sup>5</sup>, A. Ferrero<sup>2</sup>, L. Ferrero<sup>2</sup>, M. Finger<sup>6</sup>, M. Finger<sup>7</sup>, V. Frolov<sup>2</sup>, R. Garfagnini<sup>2</sup>, M. Giorgi<sup>13</sup>, O. Gorchakov<sup>1</sup>, A. Grasso<sup>2</sup>, V. Grebenyuk<sup>1</sup>, D. Hasch<sup>11</sup>, V. Ivanov<sup>1</sup>, A. Kalinin<sup>1</sup>, V.A. Kalinnikov<sup>1</sup>, Yu. Kharzheev<sup>1</sup>, N.V. Khomutov<sup>1</sup>, A. Kirilov<sup>1</sup>, Y. Kisselev<sup>1</sup>, E. Komissarov<sup>1</sup>, A. Kotzinian<sup>2</sup>, A.S. Korenchenko<sup>1</sup>, V. Kovalenko<sup>1</sup>, N.P. Kravchuk<sup>1</sup>, N.A. Kuchinski<sup>1</sup>, E. Lodi Rizzini<sup>4</sup>, V. Lyashenko<sup>1</sup>, V. Malyshev<sup>1</sup>, A. Maggiora<sup>2</sup>, M. Maggiora<sup>2</sup>, A. Martin<sup>13</sup>, Yu. Merekov<sup>1</sup>, A.S. Moiseenko<sup>1</sup>, V. Muccifora<sup>11</sup>, A. Olchevski<sup>1</sup>, V. Panyushkin<sup>1</sup>, D. Panziera<sup>5</sup>, G. Piragino<sup>2</sup>, G.B. Pontecorvo<sup>1</sup>, A. Popov<sup>1</sup>, S. Porokhovoy<sup>1</sup>, V. Pryanichnikov<sup>1</sup>, M. Radici<sup>14</sup>, P.G. Ratcliffe<sup>12</sup>, M.P. Rekalov<sup>10</sup>, P. Rossi<sup>11</sup>, A. Rozhdestvensky<sup>1</sup>, N. Russakovich<sup>1</sup>, P. Schiavon<sup>13</sup>, O. Shevchenko<sup>1</sup>, A. Shishkin<sup>1</sup>, V.A. Sidorkin<sup>1</sup>, N. Skachkov<sup>1</sup>, M. Slunicka<sup>7</sup>, A. Srnka<sup>9</sup>, V. Tchalyshev<sup>1</sup>, F. Tessarotto<sup>13</sup>, E. Tomasi<sup>8</sup>, F. Tosello<sup>2</sup>, E.P. Velicheva<sup>1</sup>, L. Venturelli<sup>4</sup>, L. Vertogradov<sup>1</sup>, M. Virius<sup>9</sup>, G. Zosi<sup>2</sup> and N. Zurlo<sup>4</sup>

<sup>1</sup>Dzhelepov Laboratory of Nuclear Problems, JINR, Dubna, Russia

<sup>2</sup>Dipartimento di Fisica “A. Avogadro” and INFN - Torino, Italy

<sup>3</sup>Dipartimento di Fisica Teorica and INFN - Torino, Italy

<sup>4</sup>Università and INFN, Brescia, Italy

<sup>5</sup>Università del Piemonte Orientale and INFN sez. di Torino - Italy

<sup>6</sup>Czech Technical University, Prague, Czech Republic

<sup>7</sup>Charles University, Prague, Czech Republic

<sup>8</sup>DAPNIA, CEN Saclay, France

<sup>9</sup>Inst. of Scientific Instruments Academy of Sciences, Brno, Czech Republic

<sup>10</sup>NSC Kharkov Physical Technical Institute, Kharkov, Ukraine

<sup>11</sup>Laboratori Nazionali Frascati, INFN, Italy

<sup>12</sup>Università dell’Insubria, Como and INFN sez. Milano, Italy

<sup>13</sup>University of Trieste and INFN Trieste, Italy

<sup>14</sup>INFN sez. Pavia, Italy

# Contents

<b>1</b>	<b>Introduction</b>	<b>3</b>
<b>2</b>	<b>The Physics</b>	<b>6</b>
2.1	Structure Functions . . . . .	6
2.2	Beam Energy for Drell-Yan processes . . . . .	7
2.3	Asymmetries in Drell-Yan processes . . . . .	8
2.4	Spin Asymmetries in Hyperon Production . . . . .	11
2.4.1	Advantages of the antiproton probe . . . . .	12
2.5	Single Spin Asymmetries . . . . .	12
2.6	Electromagnetic Form Factors . . . . .	13
<b>3</b>	<b>Antiproton production and experimental set-up</b>	<b>15</b>
3.1	Beam and target . . . . .	15
3.2	Instrumentation and Detectors . . . . .	16
3.3	Overview of the detector concept . . . . .	16
3.4	Summary and Conclusion . . . . .	18

# Chapter 1

## Introduction

The availability, at the new GSI facility (SIS300), of an antiproton beam with momenta larger than  $40 \text{ GeV}/c$ , that is with wave lengths smaller than  $4 \cdot 10^{-2} \text{ fm.}$ , makes possible a detailed study of the nucleon structure.

A complete description of the nucleon structure requires the knowledge of parton distributions (PD), including also the gluon distributions, at leading twist (twist 2) and next to leading order (twist3). The definition of these functions will be recalled in (Section 2.1).

These distributions can be obtained through the measurement of spin dependent cross-sections in a variety of hard processes.

The antiproton probe is an ideal tool for such studies as it can be seen looking to two fundamental Feynman diagrams describing the  $\bar{p}p$  interaction. The first of them (Figure 1.1) is proportional to  $\alpha^2$  and is the leading diagram illustrating the Drell-Yan process.

Here  $k$  and  $k'$  are the quadrimomenta of the quark  $q$  and antiquark  $\bar{q}$  annihilating into the virtual photon (with four-momentum  $q$ ) that originates the lepton pair with the invariant mass  $M$ . Therefore at leading order the Drell-Yan cross section will depend only on the quark (antiquark) distributions in the colliding hadrons and on the cross-section of the elementary  $q\bar{q} \rightarrow \gamma^*$  process.

The advantage of the Drell-Yan process versus other interactions like semi-inclusive deep inelastic scattering (SIDIS), for example, is then that in this process the spin dependent cross-sections can be expressed directly in terms of PD's and not as a convolution of PD's with quark fragmentation functions (QFF) like in the other hard processes. Therefore the interpretation of the data is simpler. Compared to other probes (like pions, for example) the antiprotons are unique as each of its valence quarks can contribute to this diagram.

Our purpose is then to exploit these advantages of the antiproton probe to measure PD's, in a complete range of the Bjorken variable  $x$ , using an antiproton beam slowly extracted from SIS300 and a polarised (both longitudinally and transversely) nucleon target. The relationship between the spin observables, that can so be measured and the PD's is given in (Section 2.3).

Of course a complete experiment would require also a polarised antiproton beam and therefore we are deeply interested to contribute to all the initiatives, to produce such beams either with the FILTEX or Stern-Gerlach method or making use of the  $\bar{\Lambda} \rightarrow \bar{p}\pi^+$  decay, that provides polarised antiprotons. However, as it will be described later on, new and important results could be already obtained, namely for transverse distributions[1],

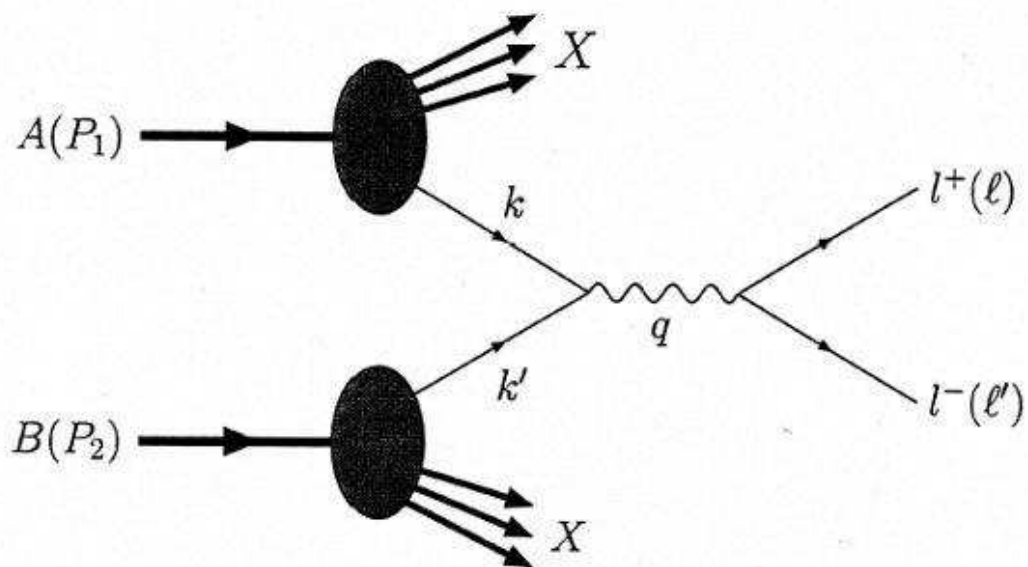


Figure 1.1: Drell-Yan dilepton production.

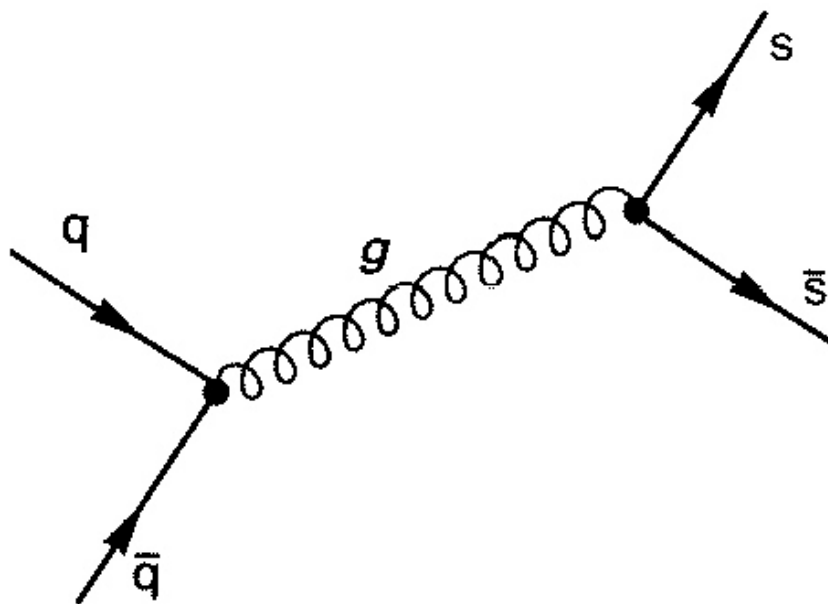


Figure 1.2: Hyperons Production

with a polarised target and unpolarised antiproton beam, provided the energy requirements for this process will be fulfilled (Section 2.2).

The second fundamental Feynman diagram, in the  $\bar{p}p$  interaction that we refer to, is illustrated in (Figure 1.2). Here too the antiproton probe is of particular interest as the correlation between the  $s$  and the  $\bar{s}$  quarks can be observed. For example, in the reaction  $\bar{p}p \rightarrow \bar{\Lambda}\Lambda$ , assuming the spin orientation of the  $\Lambda$  ( $\bar{\Lambda}$ ) is given by that of the  $s$  ( $\bar{s}$ ) quarks, the measurement, on the event by event basis, of the correlated  $\Lambda$  ( $\bar{\Lambda}$ ) polarisation will provide such correlation. The  $\Lambda$  ( $\bar{\Lambda}$ ) polarisation can be determined through the measurement of the angular distributions of  $p$  ( $\bar{p}$ ) from the weak decays  $\Lambda \rightarrow p\pi^-$  ( $\bar{\Lambda} \rightarrow \bar{p}\pi^+$ ) in the  $\Lambda$  ( $\bar{\Lambda}$ ) rest frame, that carry such information. In addition to such exclusive processes, semi-inclusive reactions like  $\bar{p}p \rightarrow \bar{\Lambda}\Lambda X$ , for example, are also accessible. From the measurement of spin dependent cross-sections of such reactions one can extract either the QFF's or the PD's. This topic will be developed in (Section 2.4).

Other important channels can be studied at the same time, measuring single spin asymmetries in semi-inclusive hadron production like in the reaction  $\bar{p}p \rightarrow \pi^+\pi^- X$  as it will be discussed in (Section 2.5).

Last but not least spin dependent measurements will allow to disentangle the electric and magnetic part of the electromagnetic form factors in the  $\bar{p}p \rightarrow l^+l^-$  reaction (Section 2.6).

# Chapter 2

## The Physics

### 2.1 Structure Functions

At the twist two level  $\mathcal{O}(1)$ , the quark structure of the nucleon[2] is described by three distribution functions. These can be also expressed in terms of the quark-nucleon forward scattering helicity amplitudes  $A(h, H \rightarrow h', H')$  where  $h$  ( $h'$ ) and  $H$  ( $H'$ ) are the helicities of the quark and of the nucleon before (after) the interaction:

1. the number density or unpolarised function,  $f_1(x)$ , that is the probability of finding a quark with a fraction  $x$  of the longitudinal momentum of the parent hadron, regardless of its spin orientation.

$$f_1(x) \propto A\left(\frac{1}{2} \frac{1}{2} \rightarrow \frac{1}{2} \frac{1}{2}\right) + A\left(\frac{1}{2} -\frac{1}{2} \rightarrow \frac{1}{2} -\frac{1}{2}\right) \quad (2.1)$$

2. the longitudinal polarisation, or helicity, distribution  $g_1(x)$ , that measures the net helicity of a quark in a longitudinally polarised hadron, that is, the number density of quarks with momentum fraction  $x$  and spin parallel to that of the hadron minus the number density of quarks with the same  $x$  but spin antiparallel.

$$g_1(x) \propto A\left(\frac{1}{2} \frac{1}{2} \rightarrow \frac{1}{2} \frac{1}{2}\right) - A\left(\frac{1}{2} -\frac{1}{2} \rightarrow \frac{1}{2} -\frac{1}{2}\right) \quad (2.2)$$

3. the transverse polarisation distribution  $h_1(x)$ , that, in a transversely polarised hadron, is the number density of quarks with momentum fraction  $x$  and polarisation parallel to that of the hadron minus the number density of quark with the same  $x$  and antiparallel polarisation.

$$h_1(x) \propto A\left(-\frac{1}{2} \frac{1}{2} \rightarrow \frac{1}{2} -\frac{1}{2}\right) \quad (2.3)$$

If quarks were perfectly collinear the distributions  $f_1(x)$ ,  $g_1(x)$  and  $h_1(x)$  would exhaust the information on the internal dynamics of the nucleon. If we admit instead a finite quark transverse momentum  $\kappa_\perp$ , the number of distribution functions increases. At twist two ( $\mathcal{O}(1)$ ) and three ( $\mathcal{O}(1/Q)$ ) there are eight  $\kappa_\perp$ -dependent distributions. Three of them,



upon integration over  $\boldsymbol{\kappa}_\perp^2$ , yield  $f_1(x)$ ,  $g_1(x)$  and  $h_1(x)$ . Other three, called  $g_{1T}(x, \boldsymbol{\kappa}_\perp^2)$ ,  $h_{1L}^\perp(x, \boldsymbol{\kappa}_\perp^2)$  and  $h_{1T}^\perp(x, \boldsymbol{\kappa}_\perp^2)$ , disappear when the hadronic tensor is integrated over  $\boldsymbol{\kappa}_\perp$ , as is the case in DIS. Finally two T odd functions, named  $f_{1T}^\perp(x, \boldsymbol{\kappa}_\perp^2)$  and  $h_1^\perp(x, \boldsymbol{\kappa}_\perp^2)$ , are respectively the distribution functions of an unpolarised quark inside a transversely polarised parent hadron and of a transversely polarised quark inside an unpolarised parent hadron.

To describe hadron production processes, other dynamical quantities are needed: the fragmentation functions, that describe the probability for a quark, in a given polarisation state, to fragment into a hadron carrying some momentum fraction  $z$ . For them we will take the same notation as for the structure functions but using capital letters.

## 2.2 Beam Energy for Drell-Yan processes

The cross-section of the Drell-Yan reaction  $\bar{p}p \rightarrow \mu^+\mu^-X$ , for a dimuon mass  $M$ , is given by:

$$\frac{d^2\sigma}{dM^2 dx_F} = \frac{4\pi\alpha^2}{9M^2 s} \frac{1}{(x_1 + x_2)} \sum_a e_a^2 [f^a(x_1)\bar{f}^a(x_2) + \bar{f}^a(x_1)f^a(x_2)]$$

Here  $x_1 = \frac{M^2}{2P_1 \cdot q}$  ;  $x_2 = \frac{M^2}{2P_2 \cdot q}$  that, in the parton model, are fractions of the

longitudinal momenta of the hadrons  $A$  and  $B$  carried by the quark and antiquark that annihilate into the virtual photon.  $x_F = (x_1 - x_2)$  is the ratio of the longitudinal momentum of the pair to the maximum allowable momentum in the center of mass frame, and  $a$  is the quark flavour, whereas

$$\tau = x_1 x_2 = \frac{M^2}{s}.$$

The scaling properties and the kinematical behaviour of the  $\bar{p}p \rightarrow \mu^+\mu^-X$  reaction are the same as for the  $pp \rightarrow \mu^+\mu^-X$ , that has been successfully used to investigate the nucleon structure, mainly studying the  $\bar{d}/\bar{u}$  asymmetry in the nucleon sea and testing the validity of the Gottfried integral.

The DY cross-section for the  $pp \rightarrow \mu^+\mu^-X$  reaction scales as:  $d^2\sigma/d\sqrt{\tau}dx_F \propto 1/s$ . This greatly favours the lowest beam energy consistent with the selection of a dimuon pair mass, (a dimuon mass spectrum [4, 5] is shown in Figure 2.1), produced in the “safe” region. The dimuon mass region, corresponding to values of  $M$  ranging from 4 to 9  $GeV/c^2$ , that is in between the  $J/\Psi$  and  $\Upsilon$  resonance families, is called “safe” because there the dimuon spectrum is essentially continuum and there are no resonance effects to disentangle in the interpretation of the data. For masses below the  $J/\Psi$  resonance families a number of potential backgrounds makes the understanding of the continuum more complex.

The upper limit of 9  $GeV/c^2$  for  $M$  defines the value of  $s$  needed to get  $0 < \tau < 1$ , that is to cover the full kinematical range allowed for  $x_1$  and  $x_2$ . The lowest corresponding kinetic energy for the  $\bar{p}$  beam is 40 GeV. This value is a reasonable compromise between the scaling behaviour of the cross-section and the need to cover the full range of the structure functions.

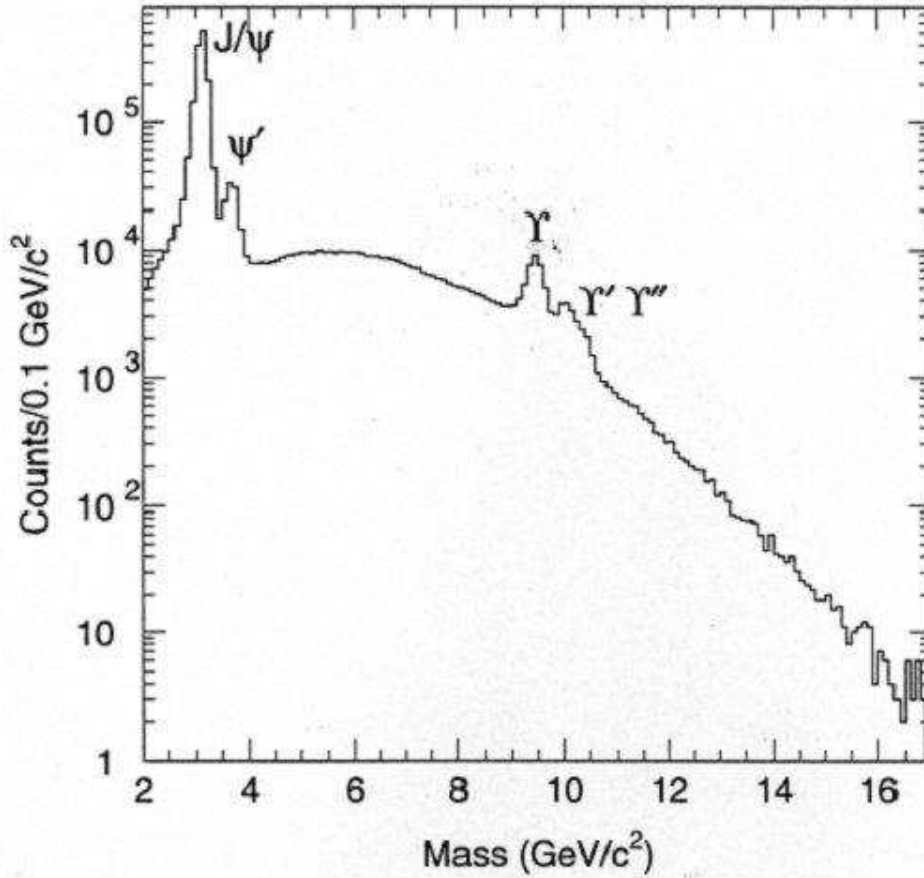


Figure 2.1: Combined dimuon mass spectrum from  $pp$  and  $pd$  collisions (from[5]).

Scaling the data of Ref. [6], where the  $\bar{p}p \rightarrow \mu^+\mu^-X$  reaction has been studied at the beam momentum of 125 GeV/c and for dimuon masses between 4 and 9 GeV/c<sup>2</sup>, we can expect an absolute cross-section, integrated over positive  $x_F$  and all transverse momenta of about 0.3 nb at 40 GeV. This value will be used to estimate the expected counting rates.

## 2.3 Asymmetries in Drell-Yan processes

The Drell-Yan process, that finds out its best expression in the  $\bar{p}p$  reaction, where all the valence quarks can contribute, favours the study of chirally odd structure functions. This because in the standard parton Drell-Yan diagram the two quarks chiralities are unrelated. Therefore there is not the chiral suppression of  $h_1(x)$ , like in DIS. This reaction is then ideal to study transversity.

If both the beam and the target could be polarised either longitudinally or transversely the observable asymmetries and their relations with the structure functions would be given by:

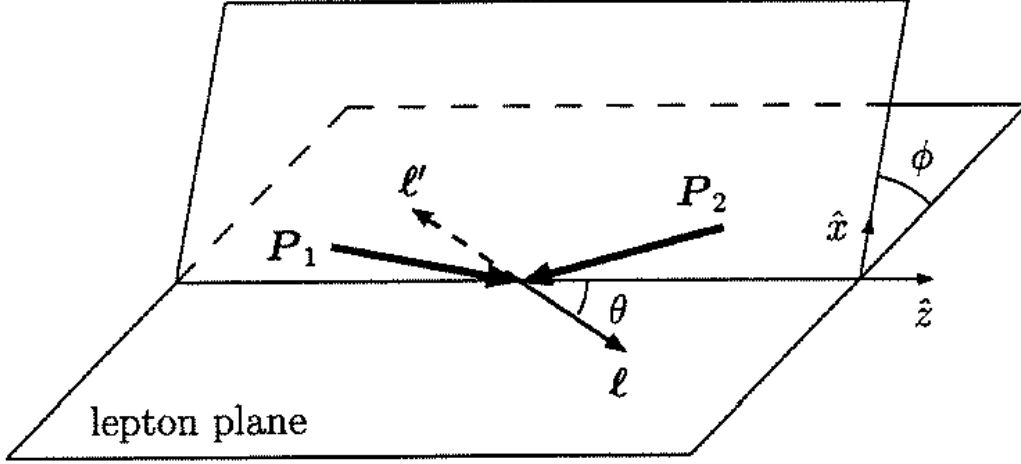


Figure 2.2: The geometry of the Drell-Yan production in the rest frame of the lepton pair.

$$A_{LL} = \frac{\sum_a e_a^2 g_1^a(x_1) g_1^{\bar{a}}(x_2)}{\sum_a e_a^2 f_1^a(x_1) f_1^{\bar{a}}(x_2)} \quad \text{for beam and target both longitudinally polarised} \quad (2.4)$$

for beam and target both transversely polarised:

$$A_{TT} = \frac{\sin^2 \theta \cos 2\phi}{1 + \cos^2 \theta} \frac{\sum_a e_a^2 h_1^a(x_1) h_1^{\bar{a}}(x_2)}{\sum_a e_a^2 f_1^a(x_1) f_1^{\bar{a}}(x_2)} \quad (2.5)$$

and if one is longitudinal and the other transverse:

$$A_{LT} = \frac{2 \sin 2\theta \cos \phi}{1 + \cos^2 \theta} \frac{M}{\sqrt{Q^2}} \frac{\sum_a e_a^2 (g_1^a(x_1) x_2 g_1^{\bar{a}}(x_2) - x_1 h_L^a(x_1) h_1^{\bar{a}}(x_2))}{\sum_a e_a^2 f_1^a(x_1) f_1^{\bar{a}}(x_2)} \quad (2.6)$$

Here the angles  $\theta$  and  $\phi$  are the polar and azimuthal angles defined in Figure 2.2. To extract the structure functions these theoretical expressions have to be compared in a fitting procedure to the experimental asymmetries measured at the same values of  $x_1(x_2)$ . These asymmetries have to be corrected by a factor  $1/(P_b \cdot f \cdot P_T)$  taking into account for the beam polarisation  $P_b$ , the dilution factor  $f$  and the target polarisation  $P_T$ . For an  $NH_3$  polarised target, the dilution factor, that is the number of polarised nucleons over the total number of nucleons in the target,  $f = 0.176$  and  $P_T = 0.85$ .

If both a polarised beam and a polarised target transversely polarised were available the Drell-Yan reaction  $\bar{p}p \rightarrow \mu^+\mu^-X$  would be the ideal tool to study transversity, that is very poorly known. This is because  $h_1^a(x)$  (see equation 2.5) has not to be unfolded with fragmentation functions, but also mainly because being a chirally odd function is not suppressed like in DIS processes. This last property is illustrated in Figure 2.3 (from Ref. [2])

However as the  $\bar{p}$  polarised beam is not yet available we have looked to alternative ways to get transverse distributions of quarks inside the nucleon.

The angular distribution of dileptons, for unpolarised beam and target is:

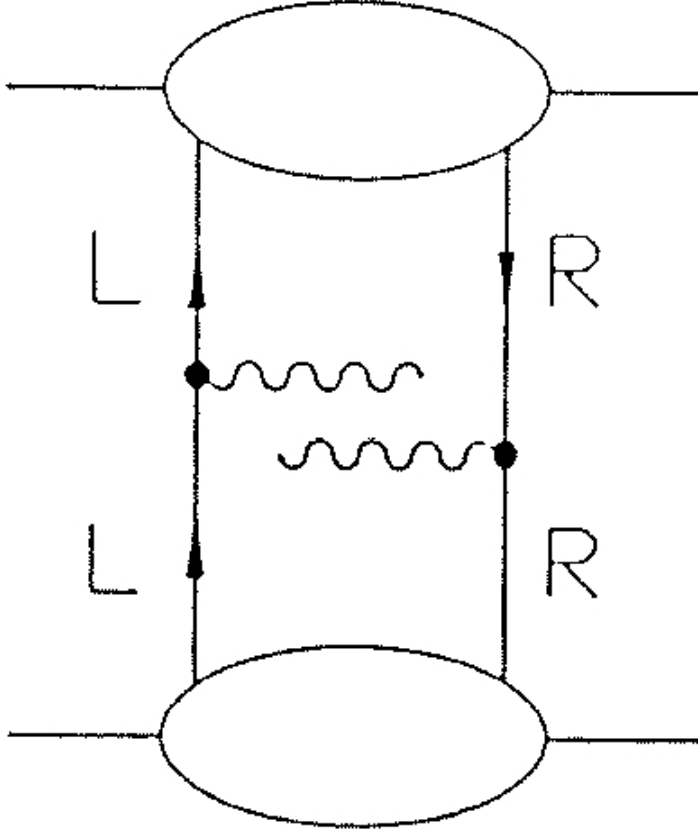


Figure 2.3: Chirality in Drell-Yan production of lepton pairs.

$$\frac{1}{\sigma} \frac{d\sigma}{d\Omega} = \frac{3}{4\pi} \frac{1}{\lambda + 3} \times (1 + \lambda \cos^2 \theta + \mu \sin^2 \theta \cos \phi + \frac{\nu}{2} \sin^2 \theta \cos 2\phi) \quad (2.7)$$

where  $\theta$  is the polar angle of the lepton in the virtual photon rest frame as defined before (see Figure 2.2).

Perturbative QCD calculations at next-to leading order give  $\lambda \approx 1$ ,  $\mu \approx 0$ ,  $\nu \approx 0$ , confirming the characteristic  $\cos^2 \theta$  distribution of the decay of a transversely polarised virtual photon, given in the parton model. However fits of experimental data (see, for example Ref. [3] show remarkably large values of  $\nu$ , reaching values of about 30%. Recently [7, 8] it has been pointed out that initial state interaction in the unpolarised Drell-Yan process could explain the observed asymmetries and be connected with the quark (anti-quark) T-odd distributions  $h_1^\perp(x_2, \boldsymbol{\kappa}_\perp^2)$  and  $\bar{h}_1^\perp(x_1, \boldsymbol{\kappa}_\perp^2)$ . Under this hypothesis, numerical estimations of the asymmetry for the  $\bar{p}p \rightarrow \mu^+\mu^-X$  process, for the maximum of  $\nu$ , of 30% are given.

The measurement of  $\cos 2\phi$  contribution to the angular distributions of the dimuon pair of the  $\bar{p}p \rightarrow \mu^+\mu^-X$  process will provide the product  $h_1^\perp(x_2, \boldsymbol{\kappa}_\perp^2) \bar{h}_1^\perp(x_1, \boldsymbol{\kappa}_\perp^2)$ . We have already proposed this measurement for the PANDA detector, where a polarised target cannot be installed because of the disturbance of the magnetic field of the solenoid. However the maximal antiproton beam energy available there limits considerably the domain of Bjorken  $x$  reachable (see Section 2.2).

If a transversely polarised hydrogen target were available, the measured asymmetry for the two target spin states depends on the  $\sin(\phi + \phi_{S_1})$  term, where  $\phi_{S_1}$  is the azimuthal angle of the target spin in the frame of Fig. 2.2. This term is  $\propto h_1(x_2, \boldsymbol{\kappa}_\perp^2) \bar{h}_1^\perp(x_1, \boldsymbol{\kappa}'_\perp{}^2)$ , as shown by[9]:

$$A_T = |S_\perp| \frac{2 \sin 2\theta \sin(\phi - \phi_{S_1})}{1 + \cos^2\theta} \frac{M}{\sqrt{Q^2}} \frac{\sum_a e_a^2 [x_1 (f_1^{a\perp}(x_1) f_1^{\bar{a}}(x_2) + x_2 h_1^a(x_1) \bar{h}_1^{\bar{a}\perp}(x_2))]}{\sum_a e_a^2 f_1^a(x_1) f_1^{\bar{a}}(x_2)} \quad (2.8)$$

This measurement, in the absence of a polarised beam, is a unique tool to probe the  $\boldsymbol{\kappa}_\perp$  dependence of quark distributions inside the nucleon.

## 2.4 Spin Asymmetries in Hyperon Production

In 1976 it was discovered that inclusively produced  $\Lambda$ 's, in unpolarized  $pp$  interactions, are negatively polarized in the direction normal to production plane. The magnitude of the polarization rises with  $x_F$  and  $p_T$  and achieves 40%. Even higher  $\Lambda$ 's polarization (60%) was obtained in exclusive reactions like  $pp \rightarrow p\Lambda K^+$ ,  $pp \rightarrow p\Lambda K^+ \pi^+ \pi^-$  etc [10, 11]. Since then this phenomenon was confirmed many times in extensive set of experiments but its theoretical explanation still remains a persisting problem.

Different quark-parton models using static SU(6) wave functions were proposed to interpret these polarization effects by introducing a spin dependence into the partonic fragmentation and recombination processes [12, 13, 14]. The  $\Lambda$  polarization is attributed to some mechanism, based on semiclassical arguments [12, 13] or inspired by QCD [14], by which produced strange quarks acquire a large negative polarization. Recently a new approach to this problem based on perturbative QCD and its factorization theorems, and which includes spin and transverse momentum of hadrons in the quark fragmentation, was proposed in [15]. These models are based on different assumptions and are able to explain the main features of the  $\Lambda$  polarization in unpolarized  $pp$ -collisions. To better distinguish between these models more complex phenomena have to be considered.

With polarized beams or target one can access new supplementary observables – the analyzing power,  $A_N$ , and the depolarization (sometime referred as spin transfer coefficient) ,  $D_{NN}$ , defined as

$$A_N = \frac{1}{P_B \cos\phi} \frac{N_\uparrow(\phi) - N_\downarrow(\phi)}{N_\uparrow(\phi) + N_\downarrow(\phi)}, \quad (2.9)$$

$$D_{NN} = \frac{1}{2P_B \cos\phi} [P_{\Lambda\uparrow}(1 + P_B A_N \cos(\phi)) - P_{\Lambda\downarrow}(1 - P_B A_N \cos(\phi))], \quad (2.10)$$

where  $\phi$  is the azimuthal angle between the beam polarization direction and the normal to scattering plane.

It is interesting to note that whereas produced  $\Lambda$  polarization remains large and negative for exclusive and inclusive channels the spin transfer coefficient is negative in low energy (beam momentum 3.67 GeV/c) exclusive production [16], compatible with zero at intermediate energies (beam momentum 13.3 and 18.5 GeV/c) [23] and positive at high energy (beam momentum 200 GeV/c) inclusive reaction [18]. Thus, the measurements at 40 GeV/c can bring an additional information on this phenomenon.

The spin dependence of exclusive annihilation reaction  $\bar{p} + p \rightarrow \bar{\Lambda} + \Lambda$  has been considered relevant to the problem of the intrinsic strangeness component of nucleon [19]-[20]. It was demonstrated [21] that the use of a transversely polarized target, in principle, allows the complete determination of the spin structure of the reaction. Corresponding measurements was performed by PS185 Collaboration, see [22] and references therein. Competing models such as  $t$ -channel meson exchange model and  $s$ -channel constituent quark model reasonably well describing the cross-section of this reaction exist. But both are unable to describe such spin observables as spin transfer from polarized proton to  $\Lambda$  ( $D_{NN}$ ) and to  $\bar{\Lambda}$  ( $K_{NN}$ ). It is evident that new data on spin transfer and correlation coefficients at higher energies and momentum transfer will be easier interpret in QCD based approaches and can help us to better understand the spin dynamics of strong interactions.

### 2.4.1 Advantages of the antiproton probe

One of the advantages of the Drell-Yan process versus other hard processes was discussed in section 2.3: in the standard parton Drell-Yan diagram the two quarks chiralities are unrelated (see Figure 2.3). Therefore there is not the chiral suppression of  $h_1(x)$ , like in DIS. A similar situation exists in the process  $\bar{p}p \rightarrow \Lambda\bar{\Lambda}X$ , described by the diagram of Figure 2.3. Here the basic diagram, illustrating the chirality conservation, is that of Figure 1.2 where a gluon replaces the  $\gamma$ . Therefore here too the two quarks chiralities are unrelated and there is not a chiral suppression of  $h_1(x)$ , like in DIS. Another advantage of the use of the antiproton beam is related to a complete correlation between the spin orientations of the  $\Lambda(\bar{\Lambda})$ .

In addition the  $\Lambda(\bar{\Lambda})$  polarisations can be easily extracted from the angular distributions of the weak decays of the  $\Lambda \rightarrow p\pi^-$  ( $\bar{\Lambda} \rightarrow \bar{p}\pi^+$ ). These decays have both a large asymmetry parameter ( $\alpha = 0.642$ ) and branching ratio ( $B.R. = 0.640$ ). Therefore, even with an unpolarised antiproton beam but with a polarised target one can get the spin correlation parameters related both to the PD's and to the QFF's.

## 2.5 Single Spin Asymmetries

The perturbative QCD spin dynamics, with the helicity conserving quark-gluon couplings, is very simple. However, such a simplicity does not appear in the hadronic spin observables; the QCD spin structure is much richer and more surprising than one could naively expect from the underlying parton dynamics. The non perturbative, long distance QCD physics has many spin properties, yet to be explored: the transverse quark spin distribution is unknown; subtle spin effects related to parton intrinsic motions in distribution functions and in fragmentation processes have been proposed and might be responsible for observed spin asymmetries; a QCD spin phenomenology seems to be possible, but more data and new measurements are crucially needed.

A typical example of such aspect of QCD is supplied by the transverse Single Spin Asymmetries (SSA),

$$A_N = \frac{d\sigma^\uparrow - d\sigma^\downarrow}{d\sigma^\uparrow + d\sigma^\downarrow},$$

measured in  $p^\uparrow p \rightarrow \pi X$  and  $\bar{p}^\uparrow p \rightarrow \pi X$  processes: the SSA at large values of  $x_F$

( $x_F \gtrsim 0.4$ ) and moderate values of  $p_T$  ( $0.7 < p_T < 2.0$  GeV/ $c$ ) have been found by several experiments [23, 24, 25] to be unexpectedly large. These asymmetries have clear features:

- the pion production at large  $x_F$  values originates from valence quarks, and indeed the sign of  $A_N$  (positive for  $\pi^+$  and negative for  $\pi^-$ ) reflects the expected sign of  $u$  and  $d$  quark polarization;
- similar values and trends of  $A_N$  have been found in experiments with center of mass energies ranging from 6.6 up to 200 GeV: this seems to hint at an origin of  $A_N$  related to fundamental properties of quark distribution and/or fragmentation.

A new experiment with anti-protons scattered off a polarized proton target, in a new kinematical region, could certainly add information on such spin properties of QCD. Also,  $A_N$  observed in  $\bar{p}p^\uparrow \rightarrow \pi X$  processes should be related to  $A_N$  observed in  $\bar{p}^\uparrow p \rightarrow \pi X$  reactions, which should be checked.

Recently, several papers have stressed the importance of measuring SSA in Drell-Yan processes [26]-[30]; these measurements allow the determination of new non perturbative spin properties of the proton, which gives the distribution of quarks in a transversely polarized proton [30]. These measurements can, at the moment, only be performed at RHIC, in the collision of transversely polarized protons on unpolarized protons; however, as it was discussed in Chapter 2, Drell-Yan processes in  $pp$  interactions, at large values of  $s$ , are much less abundant than in  $\bar{p}p$  interactions, at smaller values of  $s$ . In that the study of  $\bar{p}^\uparrow p \rightarrow \mu^+ \mu^- X$  processes at GSI offers unique possibilities.

## 2.6 Electromagnetic Form Factors

Nucleon electromagnetic form factors (FFs) in the time-like (TL) region, which can be measured through the reactions  $\bar{p}+p \leftrightarrow e^+ + e^-$ , contain important information about the nucleon structure, which can not be obtained from elastic  $eN$ -scattering, i.e in space-like (SL) region. First of all these FFs are complex functions of  $s = -q^2$ , in TL region, and analyticity allows to connect the two regions through dispersion relations.

The data about FFs in TL region, although they extend at higher  $s$ , are less precise in comparison with SL region: statistics is very low, measurements of angular distribution are very scarce and unprecise (absent for neutron), and experimental information on polarization phenomena is absent.

The reaction  $\bar{p}p \rightarrow \mu^+ \mu^-$  can be an alternative way to study FFs measuring both the angular distributions of the differential cross-sections and of the analysing power.

One can express the angular dependence of the differential cross section for  $\bar{p} + p \rightarrow \mu^+ + \mu^-$  as a function of the angular asymmetry  $\mathcal{R}$  as:

$$\frac{d\sigma}{d(\cos\theta)} = \sigma_0 [1 + \mathcal{R} \cos^2 \theta], \quad \mathcal{R} = \frac{\tau|G_M|^2 - |G_E|^2}{\tau|G_M|^2 + |G_E|^2} \quad (2.11)$$

where  $\sigma_0$  is the value of the differential cross section at  $\theta = \pi/2$ .

These quantities are very sensitive to the different underlying assumptions about the  $s$ -dependence of the FFs, therefore a precise measurement would be very interesting.

The measurement of the differential cross section for the process  $\bar{p} + p \rightarrow e^+ + e^-$  at a fixed value of  $s$  and for two different angles  $\theta$ , allowing the separation of the two FFs,

$|G_M|^2$  and  $|G_E|^2$ , is equivalent to the well known Rosenbluth separation for the elastic  $ep$ -scattering. However in TL, this procedure is simpler, as it requires to change only one kinematical variable,  $\cos\theta$ , whereas, in SL it is necessary to change simultaneously two kinematical variables: the energy of the initial electron and the electron scattering angle, fixing the momentum transfer square,  $q^2$ .

The angular dependence of the cross section, Eq. 2.11, results directly from the assumption of one-photon exchange, where the spin of the photon is equal 1 and the electromagnetic hadron interaction satisfies the  $C$ -invariance. Therefore the measurement of the differential cross section at three angles (or more) would also allow to test the presence of  $2\gamma$  exchange.

Polarization phenomena will be especially interesting in  $\bar{p}p \rightarrow \mu^+\mu^-$ . For example, the transverse polarization  $P_T$  of the proton target (or transverse polarization of the antiproton beam) results in nonzero analyzing power:

$$\mathcal{A} = \frac{\sin 2\theta \text{Im} G_E^* G_M}{D\sqrt{\tau}}, \quad D = |G_M|^2(1 + \cos^2\theta) + \frac{1}{\tau}|G_E|^2 \sin^2\theta$$

$$\frac{d\sigma}{d\Omega}(P_T) = \left(\frac{d\sigma}{d\Omega}\right)_0 [1 + \mathcal{A}P_T]$$

This analyzing power characterizes the T-odd correlation  $\vec{P} \cdot \vec{k} \times \vec{p}$ , where  $\vec{k}(\vec{p})$  is the three momentum of the  $\bar{p}$  beam (produced lepton). It is important to note that the  $\tau$ -dependence of  $\mathcal{A}$  is very sensitive to existing models of the nucleon FFs, which reproduce equally well the data in SL region.

The same information can be obtained from the final polarization in  $e^+ + e^- \rightarrow \vec{p} + \bar{p}$ , but in this case one has to deal with the problem of hadron polarimetry, in conditions of very small cross sections.

The main problems that can be solved by future measurements with a polarized antiproton beam (or an unpolarized proton beam on a polarized proton target), in view of a global interpretation of the four nucleon FFs (electric and magnetic, for neutron and proton) in TL and SL momentum transfer regions, are:

- The separation of the electric and magnetic FFs, through the angular distribution of the produced leptons: the measurement of the asymmetry  $\mathcal{R}$  (from the angular dependence of the differential cross section for  $\bar{p} + p \leftrightarrow e^+ + e^-$ ) is sensitive to the relative value of  $G_M$  and  $G_E$ .
- The presence of a large relative phase of magnetic and electric proton FF in the TL region, if experimentally proved at relatively large momentum transfer, can be considered a strong indication that these FFs have a different behavior.



# Chapter 3

## Antiproton production and experimental set-up

### 3.1 Beam and target

The announced performances of HESR give a reference antiproton beam energy of 14.5 GeV, a luminosity  $\leq 2 \times 10^{32} \text{ cm}^{-2} \text{ s}^{-1}$  and a momentum spread lower than  $\pm 1 \times 10^{-4}$ . These excellent performances do not fit with the experimental program we propose, that requires a minimal energy of 40 GeV and a limited momentum resolution. The present design of the PANDA detector, in addition, excludes the possibility to replace the internal unpolarised target with a polarised one.

We propose then to slowly extract an antiproton beam of  $\geq 40 \text{ GeV}/c$  from SIS 300 to hit an external polarised target. The expected momentum spread of such a beam should be about  $\pm 2 \times 10^{-4}$ , that is largely enough for our experiment.

To estimate the number of antiprotons that we can get from such extraction we assume the whole foreseen antiproton production accumulation rate of  $7 \times 10^{10} \bar{p}/h$  to be available and that the injection and extraction efficiencies will be always larger than 0.90. Within these assumption, we can expect a beam intensity on the target of about  $1.5 \times 10^7 \bar{p} \cdot \text{s}^{-1}$ .

For the polarised target we take as an example the polarised target system now in use in COMPASS at CERN where two cells with opposite polarisation are put one downstream of the other. This solution allows to minimize the systematic errors.

The expected luminosity will be, for a  $NH_3$  target  $10 \text{ g}/\text{cm}^2$  thick:

$$\mathcal{L} = \frac{3}{17} \times 10 \times 6 \cdot 10^{23} \times 1.5 \cdot 10^7 = 1.5 \cdot 10^{31} \text{ cm}^{-2} \text{ s}^{-1}$$

For completeness we recall that the dilution factor for such a target is  $f = 0.176$  and the polarisation  $P_T = 0.85$ .

The generation of a 40 GeV/c antiproton beam would require the following additional construction or modification items to the presently proposed configuration scheme of the new International Accelerator Facility in GSI:

1. Extraction of the accelerated anti proton beam from SIS 100 into SIS 300. Such a transition system would need to be designed and built. Or alternatively an injection scheme from the CR into the SIS 300.

2. A slow extraction system from SIS 300 into a more powerful extraction beamline able to handle momenta larger than 40 GeV/c.
3. a cave housing the experimental setup as proposed which can handle the expected radiation doses (with  $\sim 2 \times 10^7 \bar{p} \cdot s^{-1}$ ).

With this scheme, and provided that different spin orientations were available for the polarised target like in the COMPASS set-up, both longitudinal and transverse asymmetries could be measured. In addition if a transversely polarised antiproton beam could be produced and extracted from SIS 300 a unique tool for the study of the nucleon structure would be available.

An alternative solution, proposed by Hans Gutbrod, could be to imagine the HESR as a collider with both a polarised proton and antiproton beams interacting with a luminosity comparable to that reachable with an external target. If such a luminosity could be reached the advantage of such a solution would be that no dilution factor has to be considered in this case making the asymmetries measurement more precise for the same number of events collected. However to get a proton polarisation  $P_p = 0.85$  would be a difficult task to achieve. In addition only transverse asymmetries could be measured this way. The required CM energy  $\sqrt{s}$  for the proposed program could be easily reached with the present foreseen performances of HESR (15 GeV/c). In addition the higher CM energies available would allow new physics opportunities.

A polarized proton beam of up to 15 GeV/c would require a polarized proton source and an acceleration scheme preserving the polarization. No new beam line needs to be built and no additional extraction needs to be included into the acceleration system. The lattice of the HESR would have to allow an interaction region of both beams.

One of the key issues of all these proposals is the luminosity. We are aware of efforts to improve the overall antiproton production rate. We strongly support these efforts.

If the collider solution should be chosen the design of the experimental set-up would be then entirely different.

## 3.2 Instrumentation and Detectors

The proposed detector concept is inspired from the Large Angle Spectrometer, that is the first part of the COMPASS spectrometer, shown in Figure 3.1. This choice is just made to show the feasibility of the experiment with an apparatus that we know well, as a large part of us is using it now. Of course if the collider mode should become available, a different set-up should be foreseen.

## 3.3 Overview of the detector concept

The Large Angle Spectrometer consists of a large dipole magnet SM1 and various kinds of tracking detectors. SM1 is a window frame magnet with an aperture of 2.0 x 1.6 for a depth of about 1 m. It provides a field integral of about 1 Tesla m.

The tracking detectors have been chosen in such a way that they can sustain the beam rate ( $1.5 \times 10^7 \bar{p}/s$ .) and provide the hits position with such a precision to guarantee the needed resolution for the position of the vertices of the decaying particles ( $\Lambda$  and  $\bar{\Lambda}$ ) and

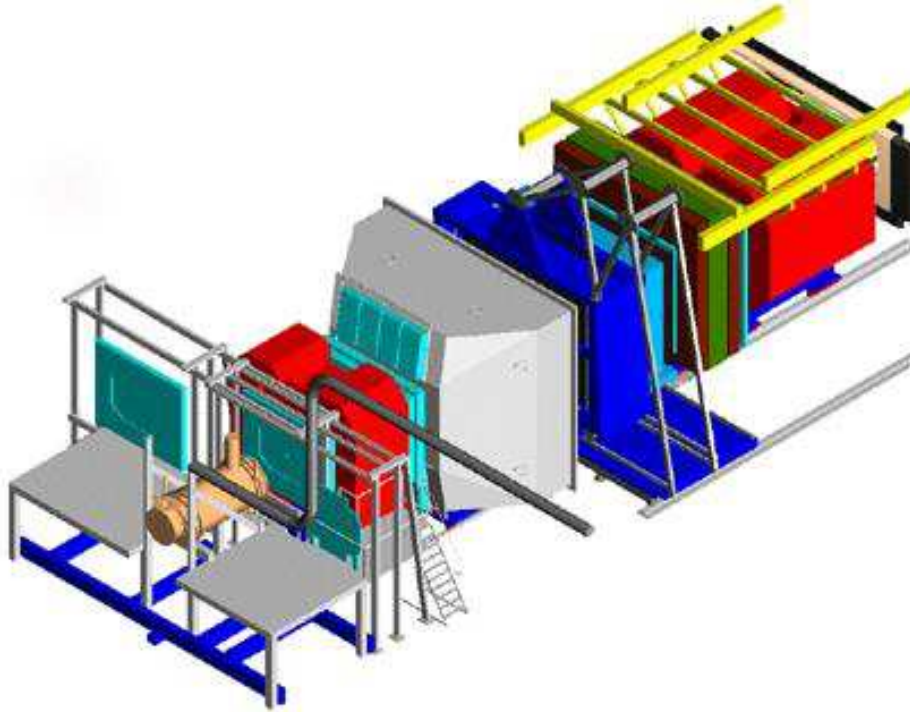


Figure 3.1: The first part of the COMPASS spectrometer.

for the widths of the corresponding peaks in the invariant mass spectra. To reach these goals and also to minimize the overall cost of the apparatus, detectors of smaller size but with thinner resolution and accepting higher rates have been chosen to detect the hits nearer to the beam trajectory. These detectors are GEM and MICROMEGAS, that provide spatial resolutions with  $\sigma \leq 70 \mu$ . To detect hits at larger distances from beam trajectories MWPC and STRAW tubes are used that provide spatial resolutions  $> 1.5$  mm. These last detectors have a dead zone in their central part, that nearer to the beam trajectories and covered by the GEM and MICROMEGAS detectors.

With this setup a mass resolution ( $\sigma \approx 2.5 \text{ MeV}/c^2$ ) can be obtained for the  $\Lambda$  ( $\bar{\Lambda}$ ).

The expected spatial resolution on the position of the decay vertices of the  $\Lambda$  ( $\bar{\Lambda}$ ) goes from  $\approx 1 \text{ cm}$ ., for very small angles with the beam trajectories, to a couple of mm. for larger angles. This spatial resolution is large enough to base the  $\Lambda$  ( $\bar{\Lambda}$ ) identification on the requirement that these vertices are outside the target.

An hodoscope of scintillators will provide the trigger with the requirement that at least two hits are present.

For the muon detection sandwiches of iron plates, IAROCCI tubes and scintillator slabs are foreseen. The scintillating slabs will provide the trigger with the requirement that two hits are present.

Finally, to minimize the background related to the interactions of the beam after the target, a vacuum pipe of growing cross-section, will catch the beam up to the beam dump. This solution, that takes advantage of the good emittance of the extracted beam, was already successfully applied in the DISTO experiment.

## 3.4 Summary and Conclusion

We hope to have underlined what a rich information on the nucleon structure could be obtained from the measurements we propose, the ideal tools being both a polarised antiproton beam and a polarised nucleon target.

As already mentioned, to get structure functions in a large  $x$  Bjorken domain the total energy in the C.M. system  $\sqrt{s}$  is a key issue. This can be obtained in two ways: either with a slow extraction from SIS300 of an antiproton beam with momenta  $\geq 40\text{GeV}/c$  (polarised?) or, as proposed by H. Gutbrod, using HESR as a collider of antiprotons (polarised?) and transversely polarised protons ( we skip here the possibility to have longitudinal polarisation ).

In the first case with a polarised target having both longitudinal and transverse polarisation available, like the COMPASS target for example, one can collect more information as discussed in Section 2.3. This will require from GSI the additional modifications discussed in Section 3.1.

The collider solution will have the advantage, for an equal luminosity, of a better factor of merit, for a proton polarisation equal to that of the target, as no dilution factor has to be taken into account in that case. The modification required by GSI are also indicated in Section 3.1.

From the detector point of view the collider solution is slightly better as a larger acceptance can be obtained. this because, the cut in acceptance for very forward (backward) emitted pairs ( of muons or Lambda's ) could be smaller.

To go further in this project, the collaboration needs to know from GSI what is feasible and discuss with the management the possible issues, once the physical case has been evaluated.

# Bibliography

- [1] V. Barone, A. Drago and P.G. Ratcliffe, Phys. Rep. 359 (2002) 1
- [2] R. Jaffe in Proc. Baryons '92, ed. M. Gai, World Scient. Singapore '93, p. 308.
- [3] J.S. Conway et al. Phys. Rev. D39 (1989) 92.
- [4] P.L. McGaughey, J.M. Moss and J.C. Peng Ann. Rev. Nucl. Part. Sci. 49 (1999) 217
- [5] E.A. Hawker *et al.* Phys. Rev. Lett. 80 (1998) 3715
- [6] E. Anassontzis *et al.* Phys. Rev. D38 (1988) 1377
- [7] D. Boer, S. Brodsky and D. Sung Hwang Phys. Rev. D67 (2003) 054003-1
- [8] J.C. Collins Phys. Lett. B536 (2002) 43
- [9] D. Boer Phys. Rev. D60 (1999) 014012
- [10] R608 Collaboration, T. Henkes *et al.*, Phys. Lett. **B283**, 155 (1992).
- [11] J. Felix *et al.*, Phys. Rev. Lett. **82**, 5213 (1999).
- [12] T.A. DeGrand and H.I. Miettinen, Phys. Rev. **D23**, 1227 (1981); **D24**, 2419 (1981); **D31**, 661(E) (1985); T. A. DeGrand, J. Markkanen, and H. I. Miettinen, *ibid.* **D32**, 2445 (1985).
- [13] B. Andersson, G. Gustafson, and G. Ingelman, Phys. Lett. **B85**, 417 (1979).
- [14] W.G.D. Dharmaratna and G.R. Goldstein, Phys. Rev. **D41**, 1731 (1990); J. Szwed, Phys. Lett. **B105**, 403 (1981);
- [15] M. Anselmino, D. Boer, U. D'Alesio and F. Murgia, Phys. Rev. **D63**, 054029 (2001).
- [16] DISTO Collaboration, F. Balestra *et al.*, Phys. Rev. Lett. **83**, 1534 (1999).
- [17] B.E. Bonner *et al.*, Phys. Rev. Lett. **58**, 447 (1987).
- [18] A. Bravar *et al.*, Phys. Rev. Lett. **78**, 4003 (1997).
- [19] M.A. Alberg, J. Ellis and D. Kharzeev, Phys. Lett. **B365**, 113 (1995).
- [20] N.K. Pak and M.P. Rekalo, Phys. Lett. **B450**, 443 (1999).
- [21] K.D. Paschke and B. Quinn, Phys. Lett. **B495**, 49 (2000).

- [22] PS185 Collaboration, K.D. Paschke *et al.*, Nucl. Phys. **A692**, 55 (2001).
- [23] K. Krueger *et al.*, Phys. Lett. **B459** (1999) 412
- [24] D.L. Adams *et al.*, Phys. Lett. **B264** (1991) 462; A. Bravar *et al.*, Phys. Rev. Lett. **77** (1996) 2626
- [25] J. Adams *et al.*, e-Print Archive: hep-ex/0310058
- [26] N. Hammon, O. Teryaev and A. Schäfer, Phys. Lett. **B390** (1997) 409
- [27] D. Boer, P.J. Mulders and O. Teryaev, Phys. Rev. **D57** (1998) 3057
- [28] D. Boer and P.J. Mulders, Nucl. Phys. **B569** (2000) 505
- [29] D. Boer and J. Qiu, Phys. Rev. **D65** (2002) 034008
- [30] M. Anselmino, U. D'Alesio and F. Murgia, Phys. Rev. **D67** (2003) 074010
- [31] M. Andreotti *et al.*, Phys. Lett B **B559**, 20 (2003) and refs therein.
- [32] O. Gayou *et al.*, Phys. Rev. Lett. **88** 092301 (2002) and refs therein.
- [33] A. Zichichi, S.M. Berman, N. Cabibbo and R. Gatto, Nuovo Cimento **XXIV** (1962) 170.
- [34] S. J. Brodsky, C. E. Carlson, J. R. Hiller and D. S. Hwang, arXiv:hep-ph/0310277.
- [35] E. Tomasi-Gustafsson and M. P. Rekalo, Phys. Lett. **504**, 291 (2001) and refs therein.
- [36] A. Z. Dubnickova, M. P. Rekalo and S. Dubnicka, Z. Phys. **C70**, 473 (1996).